Prostate Cancer Detection Using Image-Based Features in Dynamic Contrast Enhanced MRI

Wang, Liping; Zheng, Yuanjie; Rampun, Andrik; Zwiggelaar, Reyer

Published in:
Medical Image Understanding and Analysis - 25th Annual Conference, MIUA 2021, Proceedings

DOI:
10.1007/978-3-030-80432-9_4
10.1007/978-3-030-80432-9_4

Publication date:
2021

Citation for published version (APA):
Wang, L., Zheng, Y., Rampun, A., & Zwiggelaar, R. (2021). Prostate Cancer Detection Using Image-Based Features in Dynamic Contrast Enhanced MRI. In B. W. Papież, M. Yaqub, J. Jiao, A. I. Namburete, & J. A. Noble (Eds.), *Medical Image Understanding and Analysis - 25th Annual Conference, MIUA 2021, Proceedings* (Vol. 12722, pp. 43-55). (Lecture Notes in Computer Science (including subseries Lecture Notes in Artificial Intelligence and Lecture Notes in Bioinformatics); Vol. 12722 LNCS). Springer Nature. https://doi.org/10.1007/978-3-030-80432-9_4, https://doi.org/10.1007/978-3-030-80432-9_4

Prostate Cancer Detection Using Image-based Features in Dynamic Contrast Enhanced MRI

Liping Wang[1*], Yuanjie Zheng[1], Andrik Rampun[2], and Reyer Zwiggelaar[3]

[1] School of Information Science and Engineering, Shandong Normal University, China
aberwlp@sdnu.edu.cn, zhengyuanjie@gmail.com

[2] School of Medicine, Department of Infection, Immunity and cardiovascular Disease, Sheffield University, Sheffield, UK
y.rampun@sheffield.ac.uk

[3] Department of Computer Science, Aberystwyth University, Aberystwyth, UK
rrz@aber.ac.uk

Abstract. Dynamic Contrast Enhanced Magnetic Resonance Imaging (DCE MRI) provides valuable information in prostate cancer detection. Existing computer-aided detection methods focus on estimating the DCE curves as pharmacokinetic models and directly calculating the perfusion-related measurements from the DCE signals. Substantial image content contained in DCE MRI series, which captures the spatio-temporal pattern receives less attention. This work aims to investigate the performance of the image-based features extracted from DCE MRI on prostate cancer detection. Various image-based features are extracted from DCE MRI series. Their performance on prostate cancer detection is compared with features extracted from the pharmacokinetic models and the perfusion-related measurements. Features are concatenated and feature selection is applied to reduce the feature dimensionality and improve cancer detection performance. Evaluation is based on a publicly available dataset. Using image-based features outperforms using either the features extracted from the pharmacokinetic models or the perfusion-related measurements. By applying feature selection to the aggregation of all features, the performance of prostate cancer detection achieves 0.821, for the area under the receiver operating characteristics curve. This study demonstrates that compared with the commonly used pharmacokinetic models and the perfusion-related features, image-based features provide an additional contribution to prostate cancer detection and can potentially be used as an alternative approach to model DCE MRI.

Keywords: Prostate cancer detection · Image-based features · DCE MRI.

1 Introduction

Prostate cancer is the fourth most common cancer at a worldwide scale [1]. In the United States, aside from skin cancer, it remains the most frequently

* The corresponding author

diagnosed cancer affecting men and the second leading cause of death from cancer among men [2]. Prostate-specific antigen (PSA) testing and transrectal ultrasound (TRUS) guided biopsy have been widely used for prostate cancer screening. However, these techniques suffer from low accuracy, invasiveness and side effects [3].

Magnetic Resonance Imaging (MRI) has been used for non-invasive assessment of the prostate cancer since the 1980s [4]. In clinical practise, the Prostate Imaging – Reporting and Data System (PI-RADS) has been adopted for scoring the aggressiveness of the prostate cancer based on the anatomical, functional and physiologic characteristics provided by multi-parametric MRI (mpMRI), including T2-weighted (T2W), diffusion-weighted imaging (DWI) and its derivative apparent-diffusion coefficient (ADC) maps, dynamic contrast enhanced (DCE) MRI and magnetic resonance spectroscopic imaging (MRSI) [5]. In 2015, PI-RADS Version 2 was developed to promote global standardisation and diminish variation in prostate mpMRI examinations [6]. Studies have shown that integrating MRI into the standard TRUS approach benefits the tumour localisation and aggressiveness assessment from biopsy [7]. However, this process requires substantial human interaction, is time consuming and suffers from observer variability. Therefore, a computer aided prostate cancer detection system based on MRI can improve the repeatability and accuracy in carrying out biopsy, diagnosis and treatment planning.

It is notable that in PI-RADS Version 2, the role of DCE MRI becomes less important than in PI-RADS Version 1, especially for the assessment of the prostate tumour in the transition zone [6]. Nevertheless, DCE MRI possesses advantages over the other modalities – it allows image analysis in both the spatial and time domains. Studies have also shown that DCE MRI has better discrimination between cancerous and normal tissue compared to conventional T2W MRI [8]. Hence it is essential to further explore the potential of DCE MRI in prostate cancer detection in clinical practice.

In computer aided detection, DCE MRI images were quantitatively analysed by using parametric and nonparametric approaches [9, 10]. Parametric approaches aim to estimate kinetic parameters by fitting pharmacokinetic models to the concentration curves. The pharmacokinetic models proposed in the literature include Brix [11], Tofts [12], Hoffmann [13] and the phenomenological universalities (PUN) [14]. Nonparametric approaches calculate perfusion-related measurements that characterise the shape and structure of the concentration curves. The commonly used measurements include the onset time, the maximum signal intensity, wash-in rate, wash-out rate, integral under the curve and others [9, 10].

Both parametric and nonparametric approaches model DCE series by a few features/parameters for prostate cancer detection, which inevitably cause information loss. By contrast, image-based features could model substantial image content in DCE MRI images and capture both spatial and temporal enhancement patterns, which potentially benefit the prostate cancer detection. In contrast to the analysis of T2W, DWI and ADC maps, for which various image-based fea-

tures were often extracted such as the edges, statistical features, filter responses, texture descriptors and others [15, 16], the large amount of image content in DCE MRI series has not been fully taken into account for prostate cancer detection. In the literature, there have been few studies which extract image-based features from DCE MRI images for prostate cancer diagnosis. Niaf et al. extracted features such as the intensity values, texture and gradient features for prostate cancer diagnosis [17]. However, the features were extracted from only one series (i.e. one volume) of DCE MRI images and no explanation was given about why that particular series was selected. Therefore, in this study, we would like to investigate the performance of the image-based features extracted from DCE MRI on prostate cancer detection and compare the results with the commonly used parametric and non-parametric approaches.

2 Materials and Methods

2.1 Dataset

This work is based on the Initiative for Collaborative Computer Vision Benchmarking (I2CVB) dataset, which is publicly available at http://i2cvb.github.io/. It provides multi-parametric MRI data including T2W, DCE, DWI and MRSI data, acquired using a 3T whole body MRI scanner (Siemens Magnetom Trio TIM, Erlangen, Germany). The dataset consists of the MRI images taken for 17 patients who have biopsy proven prostate cancer. In our work, we only used the DCE MRI images for the prostate cancer detection experiments. T2W MRI was used for preprocessing DCE MRI images, which will be described in the following subsection. The size of the T2W MRI images ranges from $308 \times 384 \times 64$ to $368 \times 448 \times 64$ with the voxel resolution ranging between $0.68mm \times 0.68mm \times 1.25mm$ and $0.79mm \times 0.79mm \times 1.25mm$. The DCE MRI data of each patient include 40 series taken over approximately 5min; each series has 16 slices with 3.5mm slice thickness; the image size of each slice is 192×256 or 200×256 with the in-plane pixel resolution ranging between $1.09mm \times 1.09mm$ and $1.37mm \times 1.37mm$. The dataset also includes the delineations provided by an experienced radiologist. For T2W MRI, the prostate gland, the tumour region, the peripheral zone and the transition zone were annotated; for DCE MRI, only the prostate gland was annotated. Fig.1 illustrates examples of T2W and DCE MRI data from I2CVB.

2.2 Preprocessing

In order to propagate the tumours annotated on T2W to DCE images, registration was applied to align the DCE and T2W images. Normalisation was performed to reduce the inter-patient signal intensity variations due to the image acquisition process of DCE MRI. For both the registration and normalisation steps, we used the methods proposed by Lemaître [18] and the publicly available code on GitHub (https://github.com/I2Cvb/mp-mri-prostate).

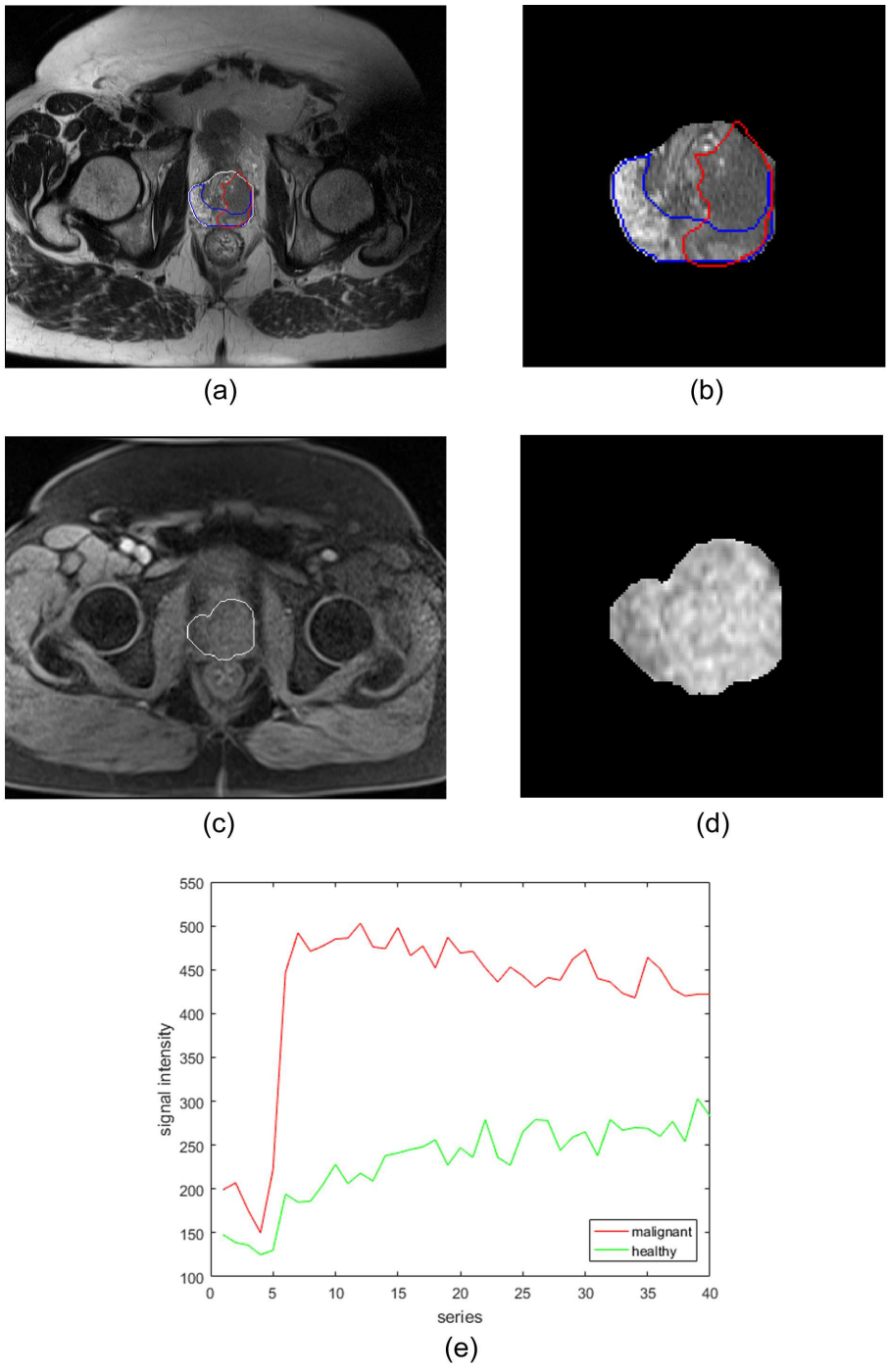

Fig. 1. (a): Example slice of T2W MRI with the prostate gland, the peripheral zone and the tumour annotated in white, blue and red contours, respectively. (b): Zoomed-in region of the prostate gland in (a). (c): Matching slice of DCE MRI with the prostate gland annotated in a white contour. (d): Zoomed-in region of the prostate gland in (c). (e): Variation of signal intensities of cancerous and healthy tissue voxels over time series in DCE MRI. The figure is better viewed in colour.

2.3 Feature Extraction

Pharmacokinetic Models Pharmacokinetic models estimate a set of parameters that reflect the physiological exchanges between vessels and extravascular extracellular space (EES) [19]. These have obtained considerable attention owing to their simplicity and small number of parameters to be estimated [9]. Brix has been one of the most commonly used models, which calculates three parameters from the DCE signal: the contrast media exchange rate k_{ep}; the elimination rate from the plasma compartment k_{el}; and an arbitrary constant simulating the tissue properties A [11]. The Hoffmann model was derived from the Brix model [12]. It redefines the constant A and the three parameters k_{ep}, k_{el} and A can also be computed. Tofts is another commonly used model, from which three parameters were calculated: the forward transfer constant of the contrast media diffusing from the blood plasma K_{trans}; the reverse constant of the contrast media returning to the blood plasma K_{ep}; and the plasma volume fraction v_p [13]. For the Tofts model, the patient-based arterial input function (AIF) signal was estimated by selecting the most enhanced voxels from the femoral and iliac arteries [20]. In addition, for the PUN model, three parameters β, a_0 and r can be calculated, where β and a_0 control the growth rate of the curve in its first part and r determines the behaviour and the speed of change of the curve in the second part [14]. The performance of the four models for prostate cancer detection were evaluated in this work.

Perfusion-related Measurements Nonparametric approaches calculate the empirical perfusion-related measurements that correlate with the physiology of the organ. These features have been commonly used because they are straightforward in definition and simple to compute [9]. We categorised these into four sets: time features, signal intensity features, derivative and integral features and ratio features as listed in Table 1.

Image-based Features DCE MRI consists of a set of T1-weighted MRI images acquired over time and hence contains substantial image information. Various image-based features can be extracted from all series of DCE MRI images such as intensity, statistical features, gradient-based features, edges, filter responses and texture descriptors.

Intensity The signal intensities of the whole time series of DCE MRI data are the most basic image information. For each voxel, the intensity values across all DCE series were used as the feature.

Statistical Features The statistical features capture the distribution of intensities within a local patch centered at each voxel. These features include mean, median, variance, standard deviation, mean of absolute deviation, median of absolute deviation, skewness, kurtosis, local contrast, local probability, 25^{th} percentile, 75^{th} percentile and others [15].

Table 1. Perfusion-related features calculated using nonparametric approaches.

Category	Symbol	Description
Time features	t_0	Onset time of the enhancement curve
	t_{max}	Time corresponding to the maximum signal intensity
	τ	Exponential time constant
Signal intensity features	S_0	Intensity at the onset of the enhancement
	S_{max}	Maximum signal intensity
	$S_{95\%}$	95% of the maximum signal intensity
	S_{end}	Signal intensity at the final time point
	S_{max} - S_0	Difference between the peak and the baseline intensities
Derivative and integral features	wash-in rate	Signal slope from t_0 to t_{max}
	wash-out rate	Signal slope from t_{max} to the final time point
	AUC	Area under the curve between t_0 and the final time point
	IAUC	Initial area under the curve between t_0 and t_{max}
	average plateau	Average signal change during the wash-out phase (from t_{max} to the final time point)
Ratio features	PER	Peak enhancement ratio calculated as $(S_{max} - S_0)/S_0$
	MITR	Maximum intensity time ratio calculated as $(S_{max} - S_0)/t_{max}$
	nMITR	Normalised MITR calculated as $(S_{max} - S_0)/(S_0 t_{max})$

Gradient-based Features Gradient-based features are able to detect the signal intensity changes and characterise micro-textures. The gradients of the image intensity computed along three dimensions, the magnitude, the gradient azimuth and elevation all belong to this category.

Edges Edges were detected by convolving edge operators like Sobel, Scharr, Prewitt and Kirsch with the original image. Phase congruency measures the significance of image features in the frequency domain [21]. It detects contrast invariant features such as the maximum moment of phase congruency covariance, the orientation image and the local weighted mean phase angle at each point in the image.

Filter Responses Gabor filters capture specific patterns of the image by tuning the scale, orientation and frequency of the kernels. The filter responses generated by convolving the Gabor filter bank with the original image were used as features. The eight maximum response (MR8) filter bank extract rotation invariant features [22]. It consists of two anisotropic filters (an edge and a bar filter at six orientations and three scales) and two isotropic filters (one Gaussian and one Laplacian of Gaussian filter). The dimensionality of the features was reduced from 38 to 8 by taking the maximum responses of the two anisotropic filters across different orientations at each scale.

Texture Descriptors Local binary patterns (LBP) describe image texture by local spatial patterns and gray level contrast [23]. It is invariant to monotonic gray

Table 2. Image-based Features.

Category	Features	Dimensionality
Intensity	signal intensities	1×40
Statistical features	mean, median, variance, standard deviation, mean of absolute deviation, median of absolute deviation, skewness, kurtosis, local contrast, local probability, 25^{th} percentile, 75^{th} percentile	12×40
Gradient-based features	gradients in three dimensions; magnitude, gradient azimuth, gradient elevation	6×40
Edges	Sobel	3×40
	Scharr	3×40
	Prewitt	3×40
	Kirsch	2×40
	Phase congruency	3×40
Filter responses	Gabor filters	6×40
	MR8 filters	8×40
Texture Descriptors	LBP	6×40
	Texton	1×40
	Tamura contrast	1×40
	Haar-like features	2×40

level changes and efficient in both computation and texture classification. In the texton-based approach, a texton dictionary was generated by applying clustering algorithms to the patches extracted from all images in the dataset. Each voxel in the image was assigned a texton identification (ID) corresponding to the closest texton in the dictionary [22]. In our work, we used texton IDs across all DCE series as the feature for each voxel [24]. Tamura contrast measures the variation of the intensity in a local region [25]. Haar-like features were calculated as the mean intensity of any cubical region or the mean intensity difference of any two random asymmetric regions within a local patch [25].

All the image-based features described above and their corresponding dimensionalities are listed in Table 2. We extracted most of the features using the parameters described in Lemaître's work [18].

Anatomical Features Five anatomical features were computed: the relative distance to the centre of the prostate, the relative distance to the contour of the prostate, the relative position in the Euclidean and cylindrical coordinate system and the zone location (i.e. the peripheral zone or the transitional zone) the voxel is in.

2.4 Classification

Leave-one-patient-out cross validation was performed in our work. A random forest classifier was adopted to classify all voxels into cancer or non-cancer. There

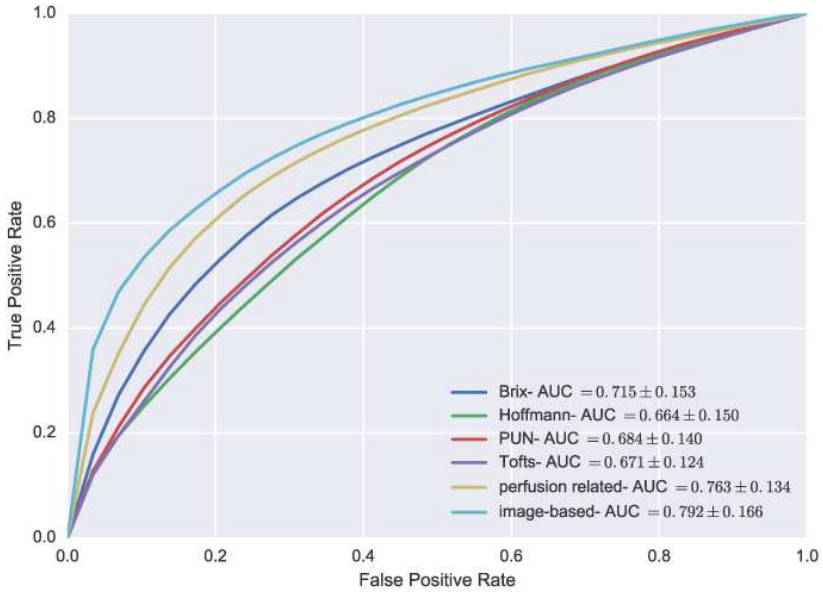

Fig. 2. Comparisons of the prostate cancer detection performance using image-based features, pharmacokinetic features and perfusion-related measurements extracted from DCE MRI. The classification performance was measured by the mean AUC value and the standard deviation over the dataset. The figure is better viewed in colour.

were 100 classifiers in the forest; the minimum number of features required to split an internal node was 2; the bootstrap samples were used when building the trees. The classification performance was evaluated by conducting a receiver operating characteristics (ROC) analysis and calculating the area under the curve (AUC) for each patient. By applying the random forest as the classifier, the importance of the features can be computed using the Gini impurity across all classifiers in the forest and the most discriminant features can be selected by setting a threshold.

3 Results

3.1 Comparison of Image-based, Pharmacokinetic and Perfusion-Related Features

We compared the prostate cancer detection performance using different categories of features extracted from DCE MRI: the image-based features, the pharmacokinetic features estimated from various models and the perfusion-related measurements. The anatomical features were always included in the evaluation of each category of features. The results shown in Fig.2 demonstrate that the Brix model outperforms the other three pharmacokinetic models in the prostate

Table 3. Classification results of using selected features from the aggregation of all features extracted from DCE MRI.

Percentile(%)	1	5	10	15	20	30	100
AUC	0.790 ± 0.157	0.816 ± 0.152	0.819 ± 0.159	0.821 ± 0.153	0.816 ± 0.157	0.813 ± 0.165	0.802 ± 0.161

cancer detection; using perfusion-related features produces better results than using the features estimated from the pharmacokinetic models; and using the image-based features results in the best classification performance.

3.2 Aggregation of All Features

All extracted features were concatenated to perform prostate cancer detection. Subsequently, percentile thresholds were set to select the most important features based on the Gini impurity values calculated in the random forest classification.

Table 3 lists the classification results generated by setting different percentiles. By contrast to the results shown in Fig.2, it can be noted that using the aggregation of all features (when the percentile equals to 100) outperforms using each individual category of features. By applying feature selection, the classification performance was further improved and the best result was obtained when 15% of the features were selected (AUC $= 0.821 \pm 0.153$).

Fig.3 illustrates the probability maps of a few cases produced by selecting the most often selected features in the leave-one-patient-out cross validation. By setting the percentile as 15%, a set of features were selected for each fold in the cross validation; all the selected features were ranked according to the times being selected during the entire cross validation process; then the features with higher rankings, which also accounts for 15% of the aggregation of all features, were used to generate the results. It can be observed that the proposed method accurately identifies the prostate cancer for cases for which the tumour exists in the peripheral zone only (a, b), in the transitional zone only (c) and in both regions (d, e). However, for the case shown in (f), the performance of prostate cancer detection was poor with lots of false positives detected.

The features used to generate the results are listed in Table 4. Most of them were selected in all folds (i.e. 17 times) in the cross validation; a few were selected in 16 or 15 folds. Features of all four categories were selected. Among all the image-based features, the statistical features and the filter responses contribute the most to the prostate cancer detection; the intensity, the gradient-based features, the edges and the texture descriptors were hardly selected.

4 Discussion

Although image-based features have been widely adopted in prostate cancer detection using MRI images like T2W, ADC and DWI, they are rarely used

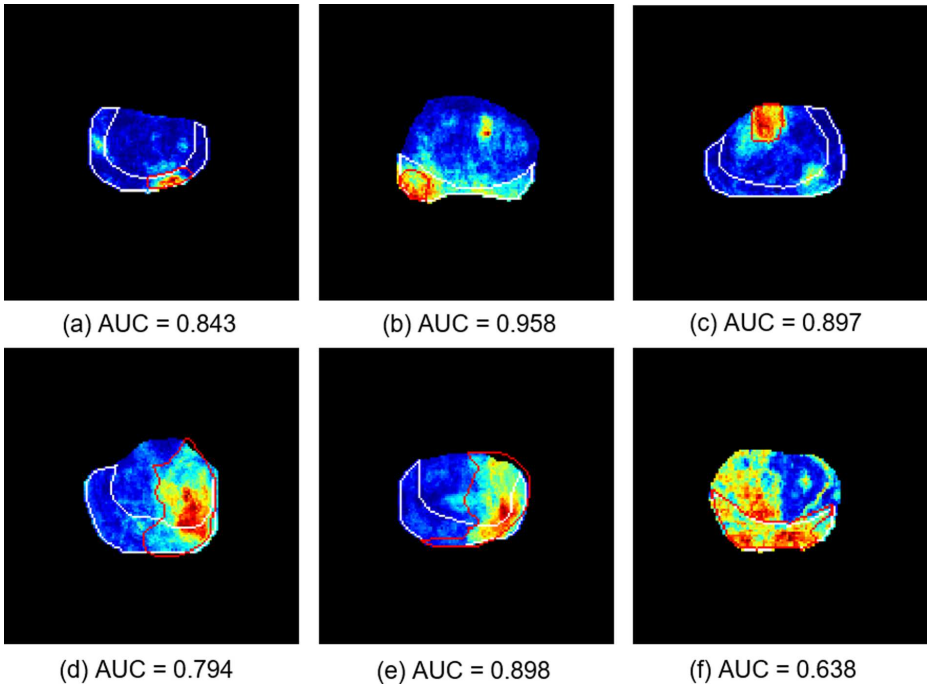

Fig. 3. Probability maps of the prostate cancer detection produced by selecting 15% of the aggregation of all features extracted from DCE MRI. Only the region of the prostate gland has been shown in these example slices of 6 different cases. The annotations of the peripheral zone and the tumour are depicted in white and red contours, respectively. The jet overlap represents the probability map of the cancer detection, where high and low probabilities of being cancer are indicated by red and blue colours, respectively. The AUC value corresponding to each case is also displayed. The figure is better viewed in colour.

to model the spatial-temporal characteristics of DCE MRI series. Experimental results have shown that compared to the commonly used approaches modelling DCE MRI series, using image-based features achieves superior performance, which indicates the additional contribution image-based features provide in prostate cancer detection.

Because all DCE MRI series were used, it was time consuming to extract various image-based features, which resulted in a high dimensionality. To mitigate this problem, a number of the most important features can be selected by applying feature selection techniques. We extracted the features with high discriminability and used them for the cancer detection.

The I2CVB dataset used in this work contains limited number of cases. However, it is the only publicly available DCE MRI prostate dataset that provides tumour segmentations. The PROSTATEx and PROSTATEx-2 challenge datasets also include DCE MRI. But these two datasets do not provide the original im-

Table 4. Selected features from the aggregation of all features.

Category	Selected Features	Dimensionality
Pharmacokinetic features	Brix model: A	1
	PUN: β	1
	Tofts: K_{trans}, K_{ep}	2
Perfusion-related features	t_{max}, S_{max}, $S_{95\%}$, S_{end} wash-in rate, IAUC, MITR	7
Image-based features	Intensity	2
	Statistical features	179
	Gradient-based features	2
	Edges	1
	Filter responses	142
	Texture descriptors	10
Anatomical features	Distance to the contour	1
	Relative Euclidean position	2
	Relative cylindrical position	3

age series but only the K_{trans} images calculated from them. And for the tumour ground truth, only the scanner coordinate position of the tumour region is provided, which makes the datasets unsuitable to investigate the performance of the spatio-temporal features contained in DCE MRI series for prostate tumour segmentation in our work.

As future work, we would like to analyse the impacts of the parameters used in feature extraction on the performance of prostate cancer detection and validate our approach on a larger dataset. We can also validate the effectiveness of the image-based features extracted from DCE MRI series on other tasks such as prostate cancer staging and Gleason grading. Based on the voxel-level classification results generated in this work, a region-level lesion segmentation and classification can be applied to remove false positives and further improve cancer detection accuracy. Moreover, instead of feeding the manually engineered features into a conventional classifier, the classification can be achieved by extracting the hierarchical features by applying deep learning algorithms. Besides of the DCE MRI, multi-parametric MRI data, such as T2W, DWI and MRSI data, can be incorporated into the approach to benefit prostate cancer detection.

5 Conclusions

This work investigated the performance of image-based features extracted from DCE MRI series on prostate cancer detection. The experimental results have demonstrated that using the image-based features outperforms other widely used approaches, such as estimating DCE signals using pharmacokinetic models and extracting perfusion-related measurements, because for image-based features substantial image information was taken into account and they can model both the spatial and temporal characteristics of the DCE series. Selecting the

most discriminant features from all categories of features reduced the feature redundancy, removed noisy information and produced excellent performance for prostate cancer detection. It has been demonstrated that apart from the commonly used features in the literature, image-based features, especially the statistical features and the filter responses, provide additional contribution for prostate cancer detection. The post-processing steps, the hierarchical features, more advanced machine learning algorithms and multi-parametric MRI can be investigated in the future to further improve prostate cancer detection.

References

1. Siegel, R., Ma, J., Zou, Z., Jemal, A.: Cancer statistics. CA: a Cancer Journal for Clinicians 2014, 64(1): 9-29.
2. Siegel, R., Naishadham, D., Jemal, A.: Cancer statistics. CA: a Cancer Journal for Clinicians 2013, 63(1): 11-30.
3. Chou, R., Croswell, JM., Dana, T., et al.: Screening for prostate cancer: a review of the evidence for the US Preventive Services Task Force. Annals of Internal Medicine 2011, 155(11): 762-771.
4. Hricak, H., Dooms, G.C., McNeal, J.E., et al.: MR imaging of the prostate gland: normal anatomy. American Journal of Roentgenology 1987, 148(1): 51-58.
5. Barentsz, J.O., Richenberg, J., Clements, R., et al.: ESUR prostate MR guidelines 2012. European Radiology 2012, 22(4): 746-757.
6. Weinreb, J.C., Barentsz, J.O., Choyke, P.L., et al.: 2016. PI-RADS Prostate Imaging-Reporting and Data System: 2015, Version 2. European Urology 2016, 69(1): 16-40.
7. Moore, C.M., Ridout, A., Emberton, M.: The role of MRI in active surveillance of prostate cancer. Current Opinion in Urology 2013, 23(3): 261-267.
8. Kim, C.K., Park, B.K., Kim. B.: Localization of prostate cancer using 3T MRI: comparison of T2-weighted and dynamic contrast-enhanced imaging. Journal of Computer Assisted Tomography 2006, 30(1): 7-11.
9. Khalifa, F., Soliman, A., El-Baz, A., et al.: Models and methods for analyzing DCE-MRI: A review. Medical Physics 2014, 41(124301).
10. Sung, Y.S., Kwon, H.J., Park, B.W., et al.: Prostate cancer detection on dynamic contrast-enhanced MRI: computer-aided diagnosis versus single perfusion parameter maps. American Journal of Roentgenology 2011, 197(5): 1122-1129.
11. Brix, G., Semmler, W., Port, R., Schad, L.R., Layer, G., Lorenz, W.J.: Pharmacokinetic parameters in CNS Gd-DTPA enhanced MR imaging. Journal of Computer Assisted Tomography 1991, 15(4): 621-628.
12. Tofts, P.S., Kermode, A.G.: Measurement of the blood-brain barrier permeability and leakage space using dynamic MR imaging. 1. Fundamental concepts. Magnetic Resonance in Medicine 1991, 17(2): 357-367.
13. Hoffmann, U., Brix, G., Knopp, M.V., et al.: Pharmacokinetic mapping of the breast: a new method for dynamic MR mammography. Magnetic Resonance in Medicine 1995, 33(4): 506-514.
14. Gliozzi, A.S., Mazzetti, S., Delsanto, P.P., Regge, D., Stasi, M.: Phenomenological universalities: a novel tool for the analysis of dynamic contrast enhancement in magnetic resonance imaging. Physics in Medicine and Biology 2011, 56(3): 573.

15. Rampun, A., Zheng, L., Malcolm, P., Tiddeman, B., Zwiggelaar, R.: Computer-aided detection of prostate cancer in T2-weighted MRI within the peripheral zone. Physics in Medicine and Biology 2016, 61(13): 4796-4825.
16. Trigui, R., Mitéran, J., Walker, P.M., Sellami, L., Hamida, A.B.: Automatic classification and localization of prostate cancer using multi-parametric MRI/MRS. Biomedical Signal Processing and Control 2017, 31: 189-198.
17. Niaf, E., Rouvière, O., Mège-Lechevallier, F., Bratan, F., Lartizien, C.: Computer-aided diagnosis of prostate cancer in the peripheral zone using multiparametric MRI. Physics in Medicine and Biology 2012, 57(12): 3833.
18. Lemaître, G.: Computer-Aided Diagnosis for Prostate Cancer using Multi-Parametric Magnetic Resonance Imaging. Doctoral dissertation 2016, Universite de Bourgogne, Universitat de Girona. p109-116.
19. Cover, T.M., Thomas, J.A.: Elements of Information Theory. John Wiley & Sons. 2006. p12-23.
20. Kybic, J., Thévenaz, P., Unser, M.: Multiresolution spline warping for EPI registration. Proceedings of the SPIE: Mathematical Imaging-Wavelet Applications in Signal and Image Processing 1999, Denver, Colorado, 3813: 571-579.
21. Scharr, H.: Optimal operators in digital image processing. Doctoral dissertation 2000. Repertus Carola University, Heidelberg, Germany.
22. Kirsch, R.A.: Computer determination of the constituent structure of biological images. Computers and Biomedical Research 1971, 4(3): 315-328.
23. Kovesi, P.: Image features from phase congruency. Videre: Journal of Computer Vision Research 1999, 1(3): 1-26.
24. Gabor, D.: Theory of communication. Part 1: The analysis of information. Journal of the Institution of Electrical Engineers-Part III: Radio and Communication Engineering 1946, 93(26): 429-441.
25. Ojala, T., Pietikäinen, M., Harwood, D.: A comparative study of texture measures with classification based on featured distributions. Pattern Recognition 1996, 29(1): 51-59.